Inorganic Chemistry

Article

pubs.acs.org/IC

Direct Synthesis of Bimetallic Pd_3Ag Nanoalloys from Bulk Pd_3Ag Alloy

Chi-Kai Lin,[†,‡] Yan-Gu Lin,[‡] Tianpin Wu,[‡] Heather M. Barkholtz,[†] Qiyin Lin,[§] Haojuan Wei,[‡] Dale L. Brewe,[∥] Jeffrey T. Miller,[‡] Di-Jia Liu,[‡] Yang Ren,[∥] Yasuo Ito,[⊥] and Tao Xu*[,†]

[†]Department of Chemistry and Biochemistry, Northern Illinois University, DeKalb, Illinois 60115, United States

[‡]Chemical Sciences and Engineering Division, Argonne National Laboratory, Argonne, Illinois 60439, United States

[§]Materials Science Division, Argonne National Laboratory, Argonne, Illinois 60439, United States

[∥]Advanced Photon Source, Argonne National Laboratory, Argonne, Illinois 60439, United States

[⊥]Department of Physics, Northern Illinois University, DeKalb, Illinois 60115, United States

Supporting Information

ABSTRACT: We report a transformative, all inorganic synthesis method of preparing supported bimetallic Pd_3Ag alloy nanoparticles. The method involves breaking down bulk Pd_3Ag alloy into the nanoparticles in liquid lithium, converting metallic Li to LiOH, and transferring Pd_3Ag nanoparticles/LiOH mixture onto non-water-soluble supports, followed by leaching off the LiOH with water under ambient conditions. The size of the resulting Pd_3Ag nanoparticles was found narrowly distributed around 2.3 nm characterized by transmission electron microscope (TEM). In addition, studies by X-ray diffraction (XRD), extended X-ray absorption fine structure (EXAFS) spectroscopy, and X-ray absorption near edge structure (XANES) spectroscopy showed that the resulting Pd_3Ag nanoparticles inherited similar atomic ratio and alloy structure as the starting material. The synthesized Pd_3Ag nanoparticles exhibited excellent catalytic activity toward hydrogenation of acrolein to propanal.

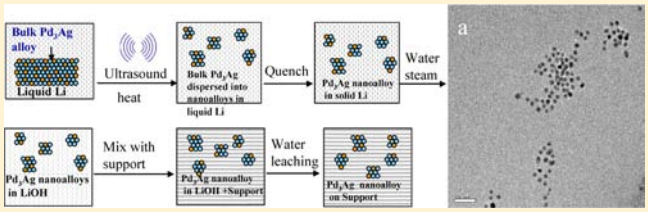

INTRODUCTION

An important method of improving the activity of heterogeneous catalyst is to replace monometallic nanoparticles with binary or multimetallic composition on various catalytic support.[1−19] Often, nanoparticles of precious metal alloys exhibit enhanced catalytic selectivity and stability over the monometallic systems. A recent study suggested that the ensemble and/or ligand effects in alloy structures could effectively suppress the formation of undesired side reactions thus enhancing the selectivity of the catalysts.[20] For example, in the case of Pd−Au alloy, isolated palladium atoms in gold with proper Pd-to-Pd distance (determined by the atomic ratio of Pd to Au) can effectively inhibit the formation of undesired byproduct in acetoxylation of ethylene to vinyl acetate.[17] Also, Ag in Pd−Ag catalyst not only increases the selectivity, stability, and lifetime in partial hydrogenation of acetylene to ethylene but also suppresses further hydrogenation of ethylene to ethane.[21−23] In these studies, the atomic intermixing of the different metal atoms was crucial to achieve the desired ensemble or ligand effects.

The state-of-the-art synthetic routes for preparing supported nanoparticles of precious metal alloys adopt a bottom-up approach. In such an approach, the mixture of the precursory metal ions and/or their ligated molecular complexes are used as the building blocks to construct the desired multimetallic nanoparticles.[2,3,15,24−28] This bottom-up method is very successful in controlling the particle size and shape by varying the concentration and the nature of the ionic metal precursors, surfactants, reducing agents, and reaction conditions (temperature, current density, etc.)[29−31] However, such an approach also introduces many intrinsic complexities. First, difference in the reduction potentials of the precursory metal ions often leads to core−shelled structures instead of the alloy structures. For example, the standard electrode potential (vs SHE) of Pd^{2+}/Pd (0.82 V) is higher than that of Ag^{2+}/Ag (0.79 V) in aqueous solution. Therefore Pd^{2+} ions are preferentially reduced before Ag^{+} ions, often resulting in the formation of the core(Pd)−shell(Ag)-like particles instead of atomically intermixed alloy.[2,32] Such process can be even more challenging when the metals have an even larger difference in the reduction potentials.[33] Additional tactics have to be applied such as annealing, selection of alternative precursors or reducing agents.[34,35] Severe particle agglomeration and support sintering may occur when the annealing has to be carried out at elevated temperature.[36,37] Unfortunately, many bulk precious metal alloys with atomically intermixed alloy structure could only be formed at extremely high temperature. For example, bulk Pd−Ag alloys are formed at temperature above 1000 °C according to the phase diagram (see Figure S1 in the Supporting

Received: September 5, 2012
Published: November 27, 2012

   dx.doi.org/10.1021/ic301940g | Inorg. Chem. 2012, 51, 13281−13288

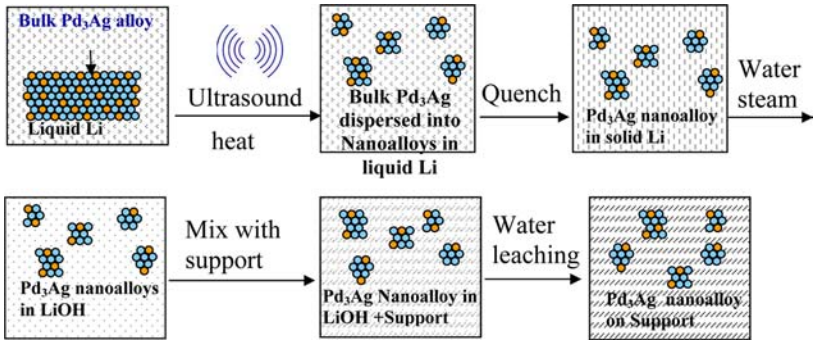

Figure 1. Schematic top-down synthesis of bimetallic Ag_3Pd alloy nanoparticles by ultrasound-assisted dispersion of the corresponding bulk Ag_3Pd alloys in liquid lithium.

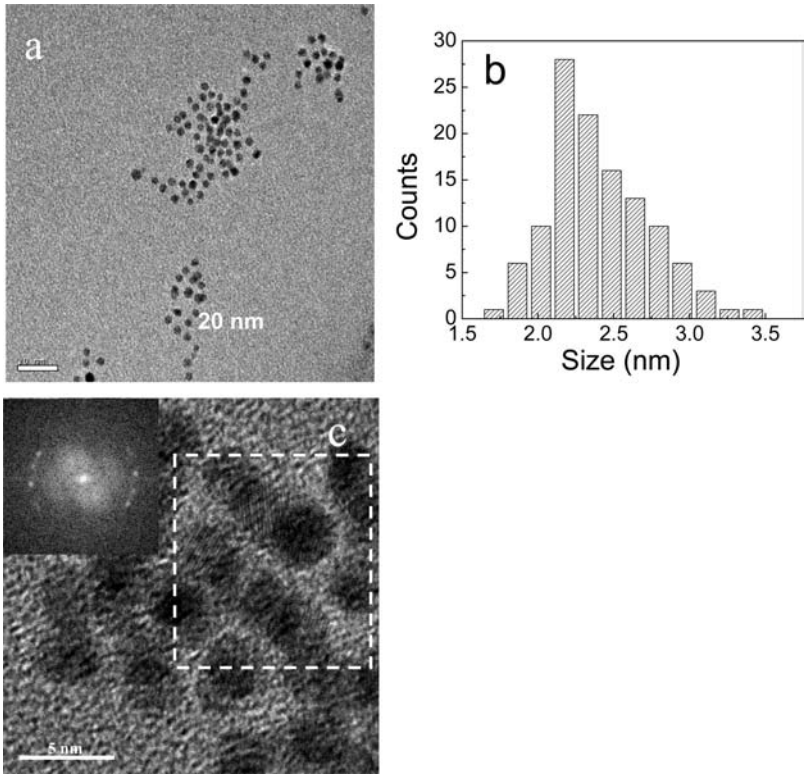

Figure 2. (a) Transmission electron micrograph (bar = 20 nm) of Pd_3Ag nanoparticles on an amorphous carbon supporting film. (b) Particle size histogram (total 117 particles). Averaged particle size is 2.3 ± 0.4 nm. (c) TEM micrograph of Pd_3Ag particles in panel a (bar = 5 nm). Some of the particles show lattice fringes of 1.96 ± 0.03 Å corresponding to the (200) reflection. The inset is an FFT of the area defined by the dashed square, indicating that the fringes appearing on all of the particles have the same lattice spacing but different orientations. The microscope magnification was calibrated with the (200) reflection of a Au standard.

Information).[38] Second, the conventional approach often requires synthesis of precursory molecules,[15] using extra stabilizing agents,[28,39,40] and an additional step to remove the organics from the process.[41] Furthermore, the ionic charges of the precursors and the support surface have to be well matched,[36,42−44] further complicating the catalyst fabrication in the laboratory and at the industrial scale.[15]

Such complications call for the development of an alternative synthetic approach for producing high-quality precious metal alloy nanoparticles with atomically intermixed structure. Moreover, the new method may generate alloy nanoparticles with unique structural and catalytic properties. In this work, we report a transformative method of producing precious metal alloy nanoparticles directly from the corresponding bulk alloy without the need of the precursor compounds. We chose Pd_3Ag as a proof-of-concept alloy and demonstrated that Pd_3Ag nanoparticles can be directly obtained by dispersing the bulk alloys in liquid Li. Liquid Li is highly corrosive to many metals. In fact, much research is dedicated to the search for liquid Li-resistant materials since lithium and its hydride are used as the coolants in nuclear reactors.[45,46] Our approach, instead, takes the advantage of the corrosive property of liquid Li to facilitate the synthesis of precious metal alloy nanoparticles.

The method is schematically illustrated in Figure 1. According to the phase diagrams of Pd−Li and Ag−Li (Figure S2 in the Supporting Information), both Pd and Ag are soluble in liquid lithium even at temperature below the lithium melting point.[47,48] Thus, we postulated that Pd_3Ag alloy could be dissolved and dispersed in lithium in the form of ultrafine nanoparticles. These nanoparticles could potentially inherit the

original atomic composition and alloy structure of the bulk Pd_3Ag alloy. After rapid quenching of the liquid Li solution, the precious metal alloy nanoparticles could be retained in the solid solution of lithium. After the lithium is converted into LiOH powder under controlled reaction with water vapor at mild temperature, the nanoparticle nuclei would be embedded in the LiOH matrix avoiding aggregation. The alloy nanoparticles in LiOH can be conveniently transferred onto any non-water-soluble support materials by simply mixing the LiOH power with the support, followed by leaching off the LiOH with excess water under ambient condition. It should be noted that safe and proper handling of Li is required due to the reactivity of lithium. This top-down method is based on a purely inorganic process with the following potential benefits: (1) The method is potentially cost competitive and environmentally friendly, as it does not use any expensive and/or toxic organic solvents or ligands and does not leave any unwanted catalyst poisoning residue such as chloride.[49,50] (2) This process does not require electrochemical reduction of metal ions, bypassing the constraint of the reduction potential by different metal ions. (3) The leaching process is under ambient conditions without the need for support pretreatment, applicable to a wide variety of support materials. (4) Li can be conveniently recycled in the form of $LiOH/Li_2O$, which are the starting materials in existing industrial production of metal lithium.[51] (5) Alloy nanoparticles prepared are already in the metallic state and require no further reduction. Such nanoparticles may have enhanced catalytic property as we will demonstrate by the current study on the notable stability of Pd_3Ag nanoparticles during hydrogenation of acrolein to propanal.

RESULTS AND DISCUSSION

Figure 2 shows the TEM images of the Pd_3Ag nanoparticles on an amorphous carbon supporting film. The Pd_3Ag nanoparticles were leached out from LiOH with water. (See Experimental Methods for details.) The distribution of the Pd_3Ag nanoparticles in Figure 2a is shown by the histogram shown in Figure 2b with the average diameter calculated to be ca. 2.3 ± 0.4 nm. The contrast variation of these nanoparticles is attributed to not only thickness (sizes) but also diffraction contrast due to the crystalline nature of the particles. A micrograph in a higher magnification of some of these particles (Figure 2c) reveals the lattice fringe of 1.96 ± 0.03 Å, i.e, a = 3.92 ± 0.06 Å. It is plausible that this may correspond to the lattice fringe of (200) reflection of the Pd_3Ag alloy since the value is between that of Pd (200) (1.945 Å) and Ag (200) (2.045 Å). The TEM results agree well with the result from the XRD and EXAFS analysis in the following section within error. The diffraction contrast of the micrographs indicates that some particles formed are single crystals while others are polycrystalline.

Figure 3 is the XRD analysis on the carbon-supported Pd_3Ag nanoparticles, in comparison with bulk Pd_3Ag macropowder, pure Pd, and carbon support. Note that the XRD of bulk Pd_3Ag (see Figure S3 in the Supporting Information) obtained from Pd_3Ag foil is not a proper comparison (in terms of relative peak intensities) with respect to the random oriented nanoparticles, because the commercial Pd_3Ag foil was mechanically rolled with preferred orientations. As such, we hand-filed a piece of Pd_3Ag foil (the same piece used for synthesis) into randomly orientated powder (macropowder) and used the XRD of the resulting Pd_3Ag macropowder in the comparison. (Two very sharp but weak peaks at 2θ = 43.9 and 75.3 in the XRD pattern

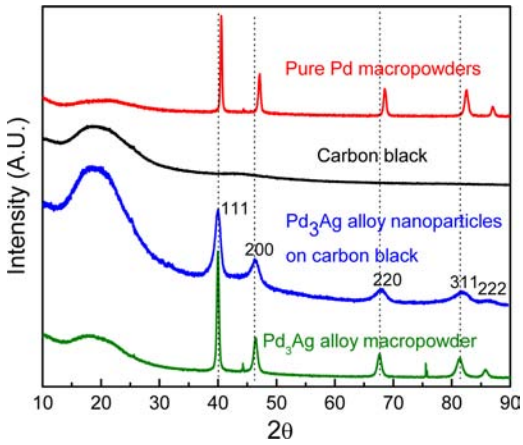

Figure 3. XRD patterns of our Pd_3Ag nanoparticles on carbon black. The Pd_3Ag macropowders are filed from their foils. The dotted lines help guide the relative peak positions of different samples. Note that the two tiny sharp peaks in the Pd_3Ag macropowder are confirmed to be artifacts due to the material from the hand file. They have nothing to do with the Pd_3Ag macropowder.

for the resulting Pd_3Ag macropowder were confirmed to be artifacts resulting from the tiny diamond grits detached off the hand-file during filing.) In comparison to bulk Pd_3Ag alloy macropowder, our Pd_3Ag nanoparticles exhibit nearly identical XRD peaks in terms of position and relative intensity, indicating that the nanoparticles obtained by this method inherit the texture of the bulk alloy. Therefore, we assign the Pd_3Ag nanoparticles we prepared as atomically intermixing alloy crystallites. On the other hand, the peaks positions of both bulk and nanoparticle Pd_3Ag notably shifted to lower 2θ values with respect to pure Pd. Since both Pd and Ag have FCC lattice, they could form a continuous series of solid solutions.[52] Because the radius of Ag (144 pm) is greater than that of Pd (137.6 pm),[53] the addition of Ag atoms into the lattice of Pd leads to the lattice expansion and, therefore, lower 2θ peak positions in XRD. The measured lattice constant is a = 3.935 Å for both Pd_3Ag nanoparticles and bulk Pd_3Ag alloy, which is in good agreement with the reported value (3.934 Å) for the bulk and larger than that of pure Pd (a = 3.886 Å).[54]

Furthermore, the diffraction pattern of pure Ag or Pd was not observed in Pd_3Ag nanoparticles. The result indicates that there is no detectable pure Ag or pure Pd phase in the resulting nanoparticles. It is also noticeable that the Pd_3Ag nanoparticles have wider diffraction peak width, from which the average grain size can be estimated using the Scherrer equation,[55] $\tau = K\lambda/(\beta \cos \theta)$, where K is the shape factor, λ is the X-ray wavelength (1.54 Å), β is the line broadening at half the maximum intensity (fwhm) in radians, and θ is the Bragg angle; τ is the mean size of the ordered (crystalline) domains. By averaging the calculated size from all five diffraction peaks, the estimated grain size of the as-synthesized Pd_3Ag nanoparticles is about 5.0 ± 1.4 nm, close to the TEM result.

We further conducted a high-resolution ($<2 \times 10^{-4}$ $\Delta Q/Q$) XRD study at 11-BM of Advanced Photon Source (APS), as is shown by Figure S4 in the Supporting Information, to verify if there is a segregated Ag phase or Pd phase in the nanoparticles. The small difference in the diffraction peak position is only distinguishable by high-resolution powder XRD. We found no split or unsymmetrical shape of peaks observed in our Pd_3Ag/C, indicating no phase segregation in our Pd_3Ag nanoparticles (blue line). For comparison, XRD of Pd_3Ag embedded in

dx.doi.org/10.1021/ic301940g | Inorg. Chem. 2012, 51, 13281−13288

LiOH (red line) is also shown, in which the sharp peaks are due to LiOH, Li_2O, and Li_3N that can all be readily leached off by water.

To verify whether the particles were truly atomically intermixed, we also conducted an EXAFS study on the as-prepared Pd_3Ag nanoparticles embedded in LiOH to investigate the local atomic environment of Pd and Ag. Pd and Ag are next to each other in the periodic table, which makes it very difficult to distinguish them from each other in the EXAFS on the basis of backscattering properties. However, Ag metal and Pd_3Ag have easily distinguishable bond distances. Figure 4a shows the Fourier transformed (FT) Ag K-edge spectrum of Pd_3Ag nanoparticles in LiOH and that of bulk Pd_3Ag foil, and Figure 4b shows a similar comparison of Pd_3Ag nanoparticles with bulk Ag. It is clear that the peak and phase positions in the FT are nearly identical between Pd_3Ag nanoparticles and the bulk, while the differences in peak magnitudes can be attributed to decreased coordination and increased disorder in the nanoparticles (see below). Furthermore, the FT of the Pd_3Ag nanoparticles shows distinct differences from the bulk Ag in both peak and phase positions. The peak position of the first shell in the nanoparticles has a smaller value of R, suggesting that the nearest neighbors to the silver atom in the nanoparticles are closer than in the bulk Ag. The comparison indicates that the Ag atoms are in an environment more like in the bulk Pd_3Ag than bulk Ag. In other words, they appear to be in an intermixed alloy similar to Pd_3Ag. Quantitative analysis of the data confirms the visual comparison of the spectra. Key results from EXAFS analyses of Pd_3Ag nanoparticles in LiOH, bulk Pd_3Ag, pure bulk Pd, and pure bulk Ag are summarized in Table 1.

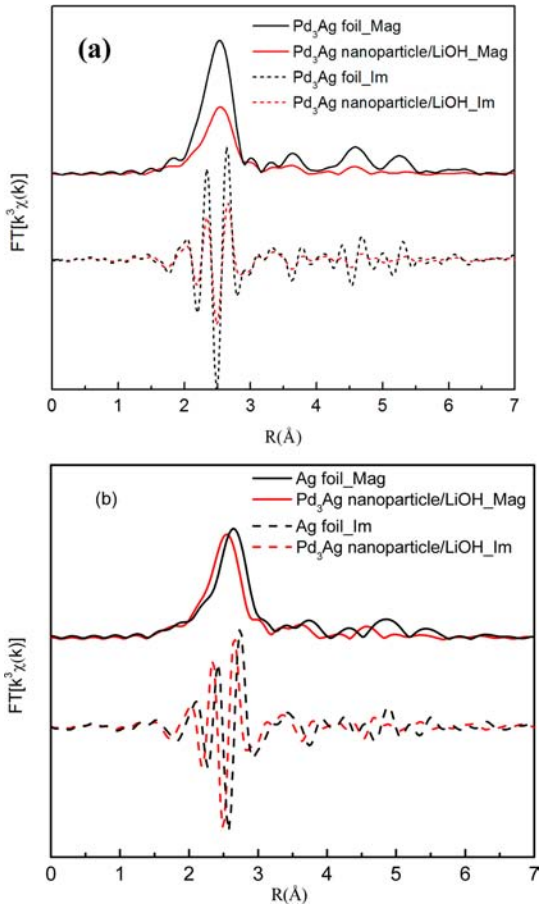

Figure 4. Fourier transformed EXAFS spectra of Pd_3Ag nanoparticles embedded in LiOH at K-edges of Ag compared to (a) bulk Pd_3Ag foil and (b) bulk Ag foil.

As seen in Table 1, the reduced effective coordination number of Ag (9.1 ± 0.5) in Pd_3Ag nanoparticles compared to that in bulk Pd_3Ag (11.6 ± 0.4) reflects the formation of nanoparticles. There are also differences in the disorder, with the nanoparticles exhibiting increased disorder compared to bulk Pd_3Ag. On one hand, the average nearest-neighbor (NN) bond distance around Ag (R = 2.788 Å) in Pd_3Ag nanoparticles is very close to that in the bulk Pd_3Ag alloy (R = 2.783 Å), but significantly shorter than that in bulk Ag (R = 2.869 Å). This result confirms the conclusion that our Pd_3Ag nanoparticles possess similar structural properties to the bulk Pd_3Ag alloy. On the other hand, the NN bond distance of the Pd atoms (R = 2.741 Å) in Pd_3Ag nanoparticles is slightly shorter that of bulk Pd_3Ag (R = 2.765 Å). This could be due to preferential enrichment of Pd atoms and/or the vacancy of Ag atoms on the surface of the nanoparticles. This trend agrees with the more reduced effective coordination number around the Pd site (8.3 ± 0.4) than that around the Ag site (9.1 ± 0.5) found in our Pd_3Ag nanoparticles. We assume that this may be ascribed to the more reduced bond length between surface Pd atoms than that between Ag atoms.[56,57]

The slight enrichment of Pd atoms in the nanoparticle surface is somewhat at variance with common expectations, where Ag has a lower surface energy[58] and a larger atomic size, both factors favoring Ag surface enrichment. Considering that the nanoparticles are not isolated during synthesis but surrounded by liquid Li, it is reasonable to assume that liquid Li plays a role to guide the atom arrangement of the nanoparticle surface. Since the Gibbs free energy of liquid Li–Pd alloy[59] is more negative than that of liquid Li–Ag alloy

Table 1. Summary of EXAFS Study on Pd_3Ag Nanoparticles (NPs) on Carbon Black and Bulk Pd_3Ag, Bulk Pd, and Bulk Ag[a]

				ΔR (Å)			
sample	edge	N	N/12	vs model	at NN	σ^2 (Å^2)	R factor
Pd_3Ag (bulk)	Pd	11.6 ± 0.5	0.97 ± 0.04	0.014 ± 0.002	2.765 ± 0.002	7.0 ± 0.2	0.0031
Pd_3Ag (bulk)	Ag	11.6 ± 0.4	0.97 ± 0.03	0.032 ± 0.002	2.783 ± 0.002	6.6 ± 0.2	0.0022
Pd (bulk)	Pd	12	1	−0.009 ± 0.002	2.742 ± 0.002	6.1 ± 0.2	0.0048
Ag (bulk)	Ag	12	1	−0.023 ± 0.001	2.869 ± 0.001	9.9 ± 0.2	0.0011
Pd_3Ag NPs	Pd	8.3 ± 0.4	0.70 ± 0.03	−0.010 ± 0.002	2.741 ± 0.002	7.4 ± 0.2	0.0024
Pd_3Ag NPs	Ag	9.1 ± 0.5	0.76 ± 0.04	0.037 ± 0.002	2.788 ± 0.002	8.9 ± 0.3	0.0034

[a]Note that, for FCC, there are 12 nearest neighbors around the selected atom. N is coordination number; R represents distance to nearest neighbor; σ is the Debye–Waller factor. The results in the table are based on a model in which each atom is surrounded by three Ag atoms and nine Pd atoms.

dx.doi.org/10.1021/ic301940g | Inorg. Chem. 2012, 51, 13281–13288

at the examined temperature,[47] the enrichment of Pd atoms on the surface of the nanoparticles prepared at 250 °C is expected.

To estimate the statistical mean particle size of the Pd_3Ag nanoparticles from EXAFS data, we employed the method described by Calvin et al.,[60] in which they assumed that the coordination numbers of spherical nanoparticles are reduced by a factor of $1 - 0.75(r/R) + 0.0625(r/R)^3$ relative to a bulk crystal, where R is the radius of the particle and r is the averaged bond length.[18] Using the nearest-neighbor bond distance and reduction in coordination number obtained from the EXAFS analysis at Ag edge, the estimated diameter of our Pd_3Ag nanoparticles in LiOH is 2.0 ± 0.3 nm, in agreement with the TEM measurement.

Further, it is necessary to confirm that the nanoparticles retain the alloy structure after transfer from LiOH to support materials. Figure 5a,b shows the Fourier transformed EXAFS

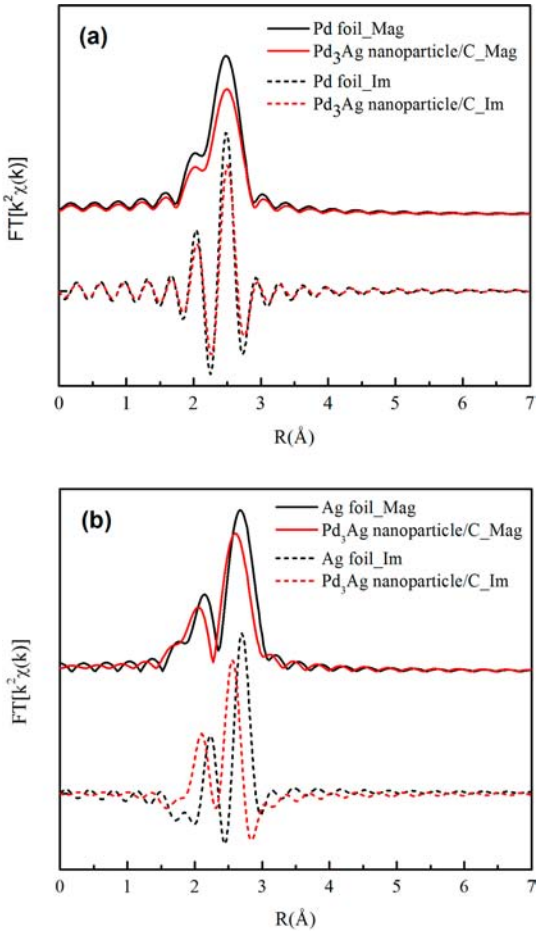

Figure 5. Fourier transformed EXAFS spectra of Pd_3Ag nanoparticles on carbon black at K-edges of (a) Pd and (b) Ag.

spectra of Pd_3Ag nanoparticles on carbon black at K-edges of Ag and Pd, respectively. It is clear that the differences between the nanoparticles and bulk Ag persist after transfer to carbon black, confirming that the alloy structure remains intact.

Differences in the EXAFS of Pd_3Ag and Pd are not so clear-cut at Pd K-edge compared to that in Ag K-edge because that Pd represents the major constituent and dominates the local structure of the alloy. However, Pd XANES (Figure 6) shows small but important changes in the shape indicative of alloy formation. The edge energy is shifted to lower energy by 1.1 eV

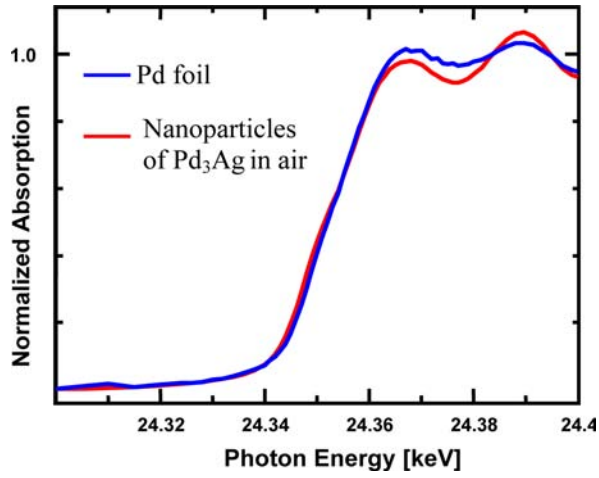

Figure 6. XANES of a pure bulk Pd foil (reduced in H_2) and our Pd_3Ag nanoparticles in air.

(24.3500 keV vs 24.3489 keV for Pd foil and Pd_3Ag/C, respectively) and the intensity of the first peak XANES is slightly lower for Pd_3Ag/C with respect to pure bulk Pd. This provides one more indication that the nanoparticles exist in the alloy structure.

It is known that nanosized Pd is easily oxidized in air at room temperature,[61,62] which may deteriorate its catalytic activity. Such oxidation can be detected by X-ray absorption near-edge structure (XANES) even with a monolayer Pd−O.[63] Oxidized Pd, i.e., PdO, has an edge energy higher than that of Pd foil (24.3500 vs 24.3545, respectively, or a 4.5 eV shift from Pd^0 to Pd^{2+}) and has a much higher XANES intensity between 24.36 and 24.39 keV than metallic Pd. The absorption edge of XANES for pure Pd nanoparticles in air differs notably from that after reduction by H_2.[63] As such, we further analyzed the XANES of our Pd_3Ag alloy nanoparticles. The blue line in Figure 7 shows the XANES of our Pd_3Ag nanoparticles

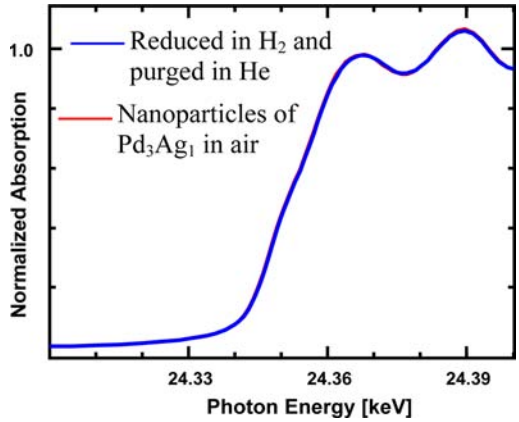

Figure 7. Pd K-edge XANES of our Pd_3Ag nanoparticles before and after reduction.

supported on carbon black after 3-month exposure in ambient air, and the redline shows the XANES measured on the same sample after in situ reduction by H_2. The two spectra overlap nearly perfectly, indicating that there is no detectable oxidation (by means of XANES) on our Pd_3Ag nanoparticles. There are also no Pd−O peaks in the EXAFS spectrum (not shown). In addition, as shown in Figure 6, the XANES of Pd_3Ag

nanoparticles matches well with that of pure metallic Pd, indicating that Pd in Pd_3Ag is metallic Pd. Theory has suggested that, by doping of Ag in Pd, the d-band of Pd shifts away from its Fermi level, which significantly weakens the chemisorption of molecules on Pd and decreases the desorption energy barrier.[64] In perspective, the room temperature oxidation-inert property found in our Pd_3Ag nanoparticles implies a good stability of the catalyst.

The catalytic activity of the Pd_3Ag nanoalloys supported over Al_2O_3 was studied for the hydrogenation of acrolein. Commercial Pd/SiO_2sample was used for comparison. The results are summarized in Figure 8. Remarkably, the conversion

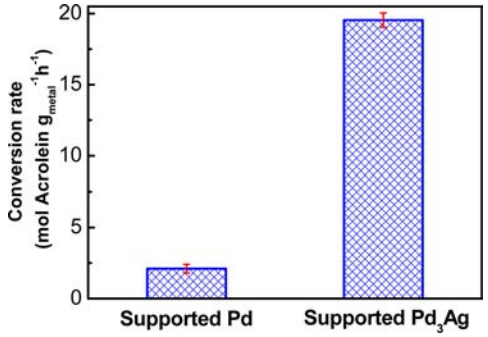

Figure 8. Catalytic activity of Pd_3Ag/Al_2O_3 in hydrogenation reaction of acrolein to propanal.

rate of acrolein over Pd_3Ag nanoalloy is nearly 10 times greater than that of monometallic Pd. The enhanced hydrogenation activity may be related to the binding energy and adsorption geometry of acrolein on Pd_3Ag bimetallic surface. Supposedly, the presence of weaker binding energies of acrolein through preferred adsorption configuration on Pd_3Ag bimetallic surfaces appears to be responsible for the enhancement in the hydrogenation reaction. The Pd_3Ag bimetallic nanoalloys may affect acrolein adsorption geometry: enhancing the interaction between acrolein molecule and the electroactive Pd_3Ag surface, which leads to the enhanced conversion toward the formation of propanal. Similar inferences have been made in the current study for the higher hydrogenation activity of acrolein by taking advantage of the synergistic effects of using bimetallic catalysts.[65] These results indicate that the as-prepared Pd_3Ag nanoparticles, without any further cleaning or calcination treatment, are readily catalytically active.

In summary, we demonstrated a novel methodology for synthesis of bimetallic Pd_3Ag alloy nanocatalysts by directly dispersing bulk Pd_3Ag in liquid lithium. After converting Li to LiOH powder followed by mixing with support materials, the Pd−Ag nanoparticles can be transferred to any water insoluble substrate by selectively leaching off the LiOH with water under ambient conditions. TEM study suggests that the particle size is around 2.3 nm. X-ray diffraction and absorption investigations suggest that the resulting Pd_3Ag nanoparticles possess an alloy structure similar to the bulk counterpart. Since nearly all precious metals are fairly soluble in liquid Li, this method provides a simple and robust alternative to wet chemistry based methods. In perspective, this method is potentially cost competitive and environmentally friendly, as it uses no organic solvents, stabilizing agents, or toxic chemicals, leading to a greener process and a smaller carbon footprint overall. The method is also versatile and applicable over a much wider range of support materials as long as they are water insoluble. In addition, these alloy catalysts could display novel redox and catalytic properties, which are critical for development of the next generation of industrial catalysts.

EXPERIMENTAL METHODS

1. Sample Preparation. The synthesis of the Li−Pd−Ag solid solution was conducted in an argon-filled glovebox (oxygen level <0.3 ppm), similar to the Li-assisted syntheses of monometallic Pt and Pd nanoparticles.[66,67] 0.5 g of lithium (99.9%, Alfa-Aesar) was placed in a nickel crucible and heated to 250 °C. As the solid lithium melted, 0.2 g of Pd_3Ag foil (99.99%, Alfa-Aesar) was added into the molten lithium. The Li−Pd_3Ag mixture was heated at 250 °C for 4 h. During heating, the surface of the liquid remained mirror-shiny all the time. To ensure the uniformity, the liquid was further ultrasonicated with a homogenizer equipped with a titanium tip (Sonozap) for 30 min. We think sonication helps the dispersion of the bulk Pd_3Ag alloy into nanoparticles and prevents particles from precipitation and reaggregation due to gravity in molten Li. The hot liquid was then quenched by quickly pouring it onto a clean 316 stainless steel plate to avoid segregation of components. The solid solution Pd_3Ag in solid liquid (equivalent to 13.5 wt % Pd_3Ag) was cut into thin pieces and placed in a water stream at 100 °C. The resulting gray solid grains (containing Pd ∼ 3.22 wt %, Ag ∼ 1.09 wt %) were then ground into fine powders with an agate mortar and pestle.

To prepare 15 wt % carbon-supported Pd_3Ag and 10 wt % Al_2O_3-supported Pd_3Ag, approximately 1 g of the resulting powder was mixed with 0.2443 g of carbon black (XC-72R) or with 0.3879 g of Al_2O_3 and the mixtures were further grounded by agate mortar and pestle. The grounded mixtures were leached with a large excess of water to remove the water-soluble LiOH. The samples were dried under vacuum at 100 °C.

2. Characterization. Regular powder X-ray diffraction (XRD) measurements were performed using a PANalytical X'pert PRO X'Celerator diffractometer with Cu Ka radiation (λ = 1.5406 Å). Each sample for XRD analysis was placed on a glass slide and covered with a Kapton tape. X-ray intensity data was collected over 2θ angles from 20° to 90°. It should be noted that the amorphous-like broad peak around 20° is the background signal from the Kapton tape. The high-resolution XRD study (λ = 0.41348 Å) is conducted at Sector 11BM, Advanced Photon Source (APS) of Argonne National Laboratory (ANL).

TEM samples were prepared by dissolving 2 mg of the as-prepared Pd_3Ag-containing LiOH powder in 2 mL of 50% aqueous ethanol solution to release the Pd_3Ag nanoparticles. The resulting nanoparticles were collected by dipping the TEM grid in the solution. The grids were further rinsed with water and ethanol to remove any residual LiOH, and the solvents were evaporated in air at room temperature overnight. The bright field TEM study was conducted on a JEOL 2010 high-resolution transmission electron microscopy with a thermionic emission gun at 200 kV. The sizes of nanoparticles were evaluated based on a count of about 100 nanoparticles.

The XAFS study was carried out at APS in ANL, Sectors 10 BM (Pd_3Ag on carbon support) and 20 (Pd_3Ag in LiOH), respectively. The Pd_3Ag-in-LiOH and Pd_3Ag/C powders were pressed into pellets with a thickness of 0.45 mm and a diameter of 6.6 mm. The Pd and Ag K-edge (24.350 and 25.514 keV, respectively) X-ray absorption measurements were conducted on the bending magnet beamline of the Materials Research Collaborative Access Team (MRCAT, 10-ID). Ionization chambers were optimized for the maximum current with linear response (ca. 10^{10} photons detected s^{-1}) using Ar (10% absorption) in the incident X-ray detector and transmission X-ray detectors. A third detector in the series simultaneously collected a Pd or Ag foil reference spectrum with each measurement for energy calibration. The X-ray beam was 1.5 × 0.7 mm^2, and data were collected in transmission mode. The spectra were obtained in step scan mode in about 15 min. The catalysts were reduced in a continuous-flow reactor, which consisted of a quartz tube (1 in. OD, 10 in. length) sealed with Kapton windows by 2 ultratorr fittings. A ball valve, welded to each ultratorr fitting, served as either the gas inlet

dx.doi.org/10.1021/ic301940g | Inorg. Chem. 2012, 51, 13281−13288

or outlet. Six catalysts were gently pressed into a cylindrical sample holder consisting of 6 sample wells. The catalyst thickness would give an absorbance (μx) of approximately 1.5 and an edge step ($\Delta\mu x$) of approximately 0.5. The EXAFS spectra of the catalysts were reduced in 4% H_2/He (100 mL/min) at 250 °C (measured by an internal thermocouple at the position of the samples), purged with He at 250 °C and cooled to room temperature and isolated from air exposure by flowing purified helium through a Matheson PUR-Gas Triple Purifier Cartridge. Phase shift and backscattering amplitudes were obtained from the Pd (N = 12, R = 2.75 Å) and Ag foil (N = 12, R = 2.89 Å) for Pd−Pd and Ag−Ag scattering. Standard procedures based on WINXAS 3.1 software were used to fit the XAS data. The EXAFS coordination parameters were obtained by a least-squares fit in r-space of the k^2-weighted Fourier transform data. The quality of the fits was equally good with both k^1 and k^3 weightings.

3. Hydrogenation Reaction. The hydrogenation reaction of gaseous acrolein was performed in a 1/2 in. OD stainless steel fixed-bed continuous gas flow reactor at atmosphere pressure. Mass flow controllers were used to control the gas flow. Acrolein (Fluka ≥95%) was delivered by a liquid pump (VICI M6), evaporated, and carried in to the system by reaction feed gas (argon and hydrogen). The molar ratio of H_2 to acrolein is held constant at 20:1 unless otherwise noted. 10 mg of catalyst was used for each test. Catalyst samples were first reduced in 20% H_2/Ar flow at 200 °C for an hour. The reaction temperature and total pressure were 200 °C and 0.1 MPa, respectively. The concentration of 3.5% acrolein was used in the reaction mixture with a flow rate of 40 sccm. The reactor effluent was analyzed by online gas chromatography (Agilent 6890) equipped with a dual column formed by an Rt-Msieve 5A and an Rt-QPLOT (Restek) for lighter gaseous species and an EC-Wax (Alltech) for less volatile species such as alcohols. TCD (thermal conductive detector) and FID (flame ionization detector) were both used for detecting H_2 and other organic/flammable compounds, respectively. A trap was installed at the end of the stream to collect condensed products. The main product was propanal in our hydrogenation reaction. The whole system was built with stainless steel parts and was heat-traced to avoid condensation of any product. The Pd and Pd_3Ag were at the same loading and particle size. The results are normalized by metal content. For an accurate comparison with commercial supported Pd catalyst, the exact same H_2-reduction pretreatment on both of the catalysts was applied prior to the catalytic reaction. In addition, the support effect between SiO_2 and Al_2O_3 in this reaction is minor and no significant difference could be observed.

■ ASSOCIATED CONTENT

Ⓢ Supporting Information

Phase diagrams of Pd−Ag, Li−Ag, and Ag−Li systems, XRD of Pd_3Ag foil, and high-resolution XRD of Pd_3Ag nanoparticles. This material is available free of charge via the Internet at http://pubs.acs.org.

■ AUTHOR INFORMATION

Corresponding Author

*E-mail: txu@niu.edu.

Notes

The authors declare no competing financial interest.

■ ACKNOWLEDGMENTS

We thankfully acknowledge support by the U.S. Department of Energy under Contract No. DE-AC02-06CH11357. T.X. also acknowledges the support from National Science Foundation (CBET-1150617) and NIU-Argonne NanoScience Graduate Fellowship. PNC/XOR facilities at the Advanced Photon Source, and research at these facilities, are supported by the U.S. Department of Energy—Basic Energy Sciences, a Major Resources Support grant from NSERC, the University of Washington, Simon Fraser University, and the Advanced Photon Source. Use of the Advanced Photon Source is also supported by the U.S. Department of Energy, Office of Science, Office of Basic Energy Sciences, under Contract DE-AC02-06CH11357. MRCAT operations are supported by the Department of Energy and the MRCAT member institutions. A portion of this work (T.W. and J.T.M.) is supported as part of the Institute for Atom-efficient Chemical Transformations (IACT), an Energy Frontier Research Center funded by the U.S. Department of Energy, Office of Science, Office of Basic Energy Sciences. Y.-G.L. was supported by the Dragon's Gate Program. The electron microscopy was conducted at the Electron Microscopy Center for Materials Research at Argonne National Laboratory, a U.S. Department of Energy Office of Science Laboratory operated under Contract No. DE-AC02-06CH11357 by UChicago Argonne, LLC.

■ REFERENCES

(1) Schmid, G.; Lehnert, A.; Malm, J.-O.; Bovin, J.-O. *Angew. Chem., Int. Ed.* **1991**, *30* (7), 874−876.
(2) Ferrando, R.; Jellinek, J.; Johnston, R. L. *Chem. Rev.* **2008**, *108*, 846−910.
(3) Gates, B. C. *Chem. Rev.* **1995**, *95*, 511−522.
(4) Burda, C.; Chen, X.; Narayanan, R.; El-Sayed, M. A. *Chem. Rev.* **2005**, *105* (4), 1025−1102.
(5) Teschner, D.; Vass, E.; Hävecker, M.; Zafeiratos, S.; Schnörch, P.; Sauer, H.; Knop-Gericke, A.; Schlögl, R.; Chamam, M.; Wootsch, A.; Canning, A. S.; Gamman, J. J.; Jackson, S. D.; Mcgregor, J.; Gladden, L. F. *J. Catal.* **2006**, *242*, 26−37.
(6) Lahiri, D.; Bunker, B.; Mishra, B.; Zhang, Z.; Meisel, D.; Doudna, C. M.; Bertino, M. F.; Blum, F. D.; Tokuhiro, A. T.; Chattopadhyay, S.; Shibata, T.; Terry, J. *J. Appl. Phys.* **2005**, *97* (9), 094304−8.
(7) Roth, C.; Papworth, A. J.; Hussain, I.; Nichols, R. J.; Schiffrin, D. J.; Pt/Ru, A. *J. Electroanal. Chem.* **2005**, *581* (1), 79−85.
(8) Goodenough, J. B.; Hamnett, A.; Kennedy, B. J.; Manoharan, R.; Weeks, S. A. *J. Electroanal. Chem. Interfacial Electrochem.* **1988**, *240* (1−2), 133−145.
(9) Wang, W. H.; Cao, G. Y. *J. Nanopart. Res.* **2007**, *9*, 1153−1161.
(10) Wang, C.; van der Vliet, D.; Chang, K.-C.; You, H.; Strmcnik, D.; Schlueter, J. A.; Markovic, N. M.; Stamenkovic, V. R. *J. Phys. Chem. C* **2009**, *113* (45), 19365−19368.
(11) Zhu, J.; Cheng, F.; Tao, Z.; Chen, J. *J. Phys. Chem. C* **2008**, *112* (16), 6337−6345.
(12) Doudna, C. M.; Bertino, M. F.; Tokuhiro, A. T. *Langmuir* **2002**, *18* (6), 2434−2435.
(13) Huang, C.-Y.; Chiang, H.-J.; Huang, J.-C.; Sheen, S.-R. *Nanostruct. Mater.* **1998**, *10* (8), 1393−1400.
(14) Alayoglu, S.; Nilekar, A. U.; Mavrikakis, M.; Eichhorn, B. *Nat. Mater.* **2008**, *7*, 233−238.
(15) Kettler, P. B. *Org. Process Res. Dev.* **2003**, *7*, 342−354.
(16) Remita, S.; Mostafavi, M.; Delcourt, M. O. *Radiat. Phys. Chem.* **1996**, *47* (2), 275−279.
(17) Chen, M. S.; Kumar, D.; Yi, C. W.; Goodman, D. W. *Science* **2005**, *310*, 291−293.
(18) Stamenkovic, V. R.; Fowfer, B.; Mun, B. S.; Wang, G.; Ross, P. N.; Lucas, C. A.; Markovic, N. M. *Science* **2007**, *315*, 493−497.
(19) Noordermeer, A.; Kok, G. A.; Nieuwenhuys, B. E. *Surf. Sci.* **1986**, *165* (2−3), 375−392.
(20) Jin, Y.; Datye, A. K.; Rightor, E.; Gulotty, R.; Waterman, W.; Smith, M.; Holbrook, M.; Maj, J.; Blackson, J. *J. Catal.* **2001**, *203* (2), 292−306.
(21) Huang, D. C.; Chang, K. H.; Pong, W. F.; Tseng, P. K.; Hung, K. J.; Huang, W. F. *Catal. Lett.* **1998**, *53* (3−4), 155−159.
(22) Sales, E. A.; Benhamida, B.; Caizergues, V.; Lagier, J. P.; Fievet, F.; Bozon-Verduraz, F. *Appl. Catal., A* **1998**, *172* (2), 273−283.
(23) Zhang, Q.; Li, J.; Liu, X.; Zhu, Q. *Appl. Catal., A* **2000**, *197* (2), 221−228.
(24) Chen, C.; Akashi, M. *Langmuir* **1997**, *13*, 6465−6472.

(25) Herricks, T.; Chen, J.; Xia, Y. *Nano Lett.* **2004**, *4*, 2367−2371.
(26) Teranishi, T.; Hosoe, M.; Tanaka, T.; Miyake, M. *J. Phys. Chem. B* **1999**, *103*, 3818−3827.
(27) Yang, C.-C.; Wan, C.-C.; Wang, Y.-Y. *J. Colloid Interface Sci.* **2004**, *279* (2), 433−439.
(28) Yang, J.; Lee, J. Y.; C., D. T.; Too, H. P. *Langmuir* **2003**, *19*, 10361−10365.
(29) Reetz, M. T.; Helbig, W. *J. Am. Chem. Soc.* **1994**, *116* (16), 7401−7402.
(30) Lu, J.; Stair, P. C. *Langmuir* **2010**, *26* (21), 16486−16495.
(31) Guerrero, M.; García-Anton, J.; Tristany, M.; Pons, J.; Ros, J.; Philippot, K.; Lecante, P.; Chaudret, B. *Langmuir* **2010**, *26* (19), 15532−15540.
(32) Christensen, A.; Ruban, A. V.; Stoltze, P.; Jacobsen, K. W.; Skriver, H. L.; oslash; rskov, J. K.; Besenbacher, F. *Phys. Rev. B* **1997**, *56* (10), 5822.
(33) Toshima, N.; Yonezawa, T. *New J. Chem.* **1998**, *22* (11), 1179−1201.
(34) Phillips, J.; Auroux, A.; Bergeret, G.; Massardier, J.; Renouprez, A. *J. Phys. Chem.* **1993**, *97* (14), 3565−3570.
(35) Röder, H.; Schuster, R.; Brune, H.; Kern, K. *Phys. Rev. Lett.* **1993**, *71* (13), 2086−2089.
(36) Coloma, F.; Sepulveda-Escribano, A.; Fierro, J. L. G.; Rodriguez-Reinoso, F. *Langmuir* **1994**, *10*, 750−755.
(37) Zaragoza-Martín, F.; Sopeña-Escario, D.; Morallón, E.; Salinas-Martínez de Lecea, C. *J. Power Sources* **2007**, *171* (2), 302−309.
(38) Karakaya, I.; Thompson, W. *J. Phase Equilib.* **1988**, *9* (3), 237−243.
(39) Ahmadi, T. S.; Wang, Z. L.; Green, T. C.; Henglein, A.; El-Sayed, M. A. *Science* **1996**, *272* (5270), 1924−1925.
(40) Yang, J.; Deivaraj, T. C.; Too, H. P.; Lee, J. Y. *J. Phys. Chem. B* **2004**, *108*, 2181−2185.
(41) Salavagione, H. J.; Sanchís, C.; Morallón, E. *J. Phys. Chem. C* **2007**, *111*, 12454−12460.
(42) Amine, K.; Mizuhata, M.; Oguro, K.; Takenaka, H. *J. Chem. Soc., Faraday Trans.* **1995**, *91*, 4451−4458.
(43) Fujimoto, T.; Terauchi, S. Y.; Umehara, H.; Kojima, I.; Henderson, W. *Chem. Mater.* **2001**, *13*, 1057−1060.
(44) Solar, J. M.; y Leon, C. A. L.; Osseo-Asaret, K.; Radovic, L. R. *Carbon* **1990**, *28*, 369−375.
(45) Haertling, C. L.; Hanrahan, R. J.; Tesmer, J. R. *J. Phys. Chem. C* **2007**, *111*, 1716−1724.
(46) Vertkov, A. V.; Evtikhin, V. A.; Lyublinsk, I. E. *J. Nucl. Mater.* **1996**, *233*−*237*, 452−455.
(47) Pelton, A. D. *J. Phase Equilib.* **1986**, *7* (3), 223−228−228.
(48) Sangster, J.; Pelton, A. D. *J. Phase Equilib.* **1992**, *13* (1), 63−66.
(49) Bönnemann, H.; Brinkmann, R.; Kinge, S.; Ely, T. O.; Armand, M. *Fuel Cells* **2004**, *4* (4), 289−296.
(50) Zhao, X.; Sun, G.; Jiang, L.; Chen, W.; Tang, S.; Zhou, B.; Xin, Q. *Electrochem. Solid-State Lett.* **2005**, *8*, A149−A151.
(51) Kipouros, G. J.; Sadoway, D. R. *JOM* **1998**, *50* (5), 24−26.
(52) McKeehan, L. W. *Phys. Rev.* **1922**, *20* (5), 424−432.
(53) Ignatova, K.; Nikolova, L.; Dimov, W. *J. Phys. Chem. B* **1997**, *101* (35), 6891−6894.
(54) Coles, B. R. *Proc. Phys. Soc., London, Sect. B* **1952**, *65* (387), 221−229.
(55) Patterson, A. L. *Phys. Rev.* **1939**, *56* (10), 978−982.
(56) Fukuhara, M. *Phys. Lett. A* **2003**, *313*, 427−430.
(57) Qi, W. H.; Wang, M. P. *J. Nanopart. Res.* **2005**, *7*, 51−57.
(58) Mottet, C.; Rossi, G.; Baletto, F.; Ferrando, R. *Phys. Rev. Lett.* **2005**, *95* (3), 035501.
(59) Nohira, T.; Ito, Y. *J. Electrochem. Soc.* **1998**, *145* (3), 785−790.
(60) Calvin, S.; Luo, S. X.; Caragianis-Broadbridge, C.; McGuinness, J. K.; Anderson, E.; Lehman, A.; Wee, K. H.; Morrison, S. A.; Kurihara, L. K. *Appl. Phys. Lett.* **2005**, *87* (23), 233102-1−233102-3.
(61) Seriani, N.; Harl, J.; Mittendorfer, F.; Kresse, G. *J. Chem. Phys.* **2009**, *131*, 054701.
(62) Klikovits, J.; Napetschnig, E.; Schmid, M.; Seriani, N.; Dubay, O.; Kresse, G.; Varga, P. *Phys. Rev. B* **2007**, *76*, 045405.
(63) Ingham, B.; Hendy, S. C.; Fong, D. D.; Fuoss, P. H.; Eastman, J. A.; Lassesson, A.; Tee, K. C.; Convers, P. Y.; Brown, S. A.; Ryan, M. P.; Toney, M. F. *J. Phys. D: Appl. Phys.* **2010**, *43*, 075301.
(64) Hammer, B.; Nørskov, J. K. *Adv. Catal.* **2000**, *45*, 71−129.
(65) Murillo, L. E.; Menning, C. A.; Chen, J. G. *J. Catal.* **2009**, *268*, 335−345.
(66) Lin, C.; Xu, T.; Yu, J.; Ge, Q.; Xiao, Z. *J. Phys. Chem. C* **2009**, *113* (19), 8513−8517.
(67) Xu, T.; Lin, C.; Wang, C.; Brewe, D. L.; Ito, Y.; Lu, J. *J. Am. Chem. Soc.* **2010**, *132*, 2151−2153.